

# Parallel Ising Annealer via Gradient-based Hamiltonian Monte Carlo

Hao Wang<sup>1†</sup>, Zixuan Liu<sup>2†</sup>, Zhixin Xie<sup>3</sup>, Langyu Li<sup>3</sup>,  
Zibo Miao<sup>2\*</sup>, Wei Cui<sup>1\*</sup>, Yu Pan<sup>3\*</sup>

<sup>1</sup>School of Automation Science and Engineering, South China University of Technology, 381 Wushan Road, Guangzhou, 510641, Guangdong, China.

<sup>2</sup>School of Mechanical Engineering and Automation, Harbin Institute of Technology, Taoyuan Street, Shenzhen, 518055, Guangdong, China.

<sup>3</sup>College of Control Science and Engineering, Zhejiang University, 38 Zheda Road, Hangzhou, 310027, Zhejiang, China.

\*Corresponding author(s). E-mail(s): [miaozibo@hit.edu.cn](mailto:miaozibo@hit.edu.cn);  
[aucuiwei@scut.edu.cn](mailto:aucuiwei@scut.edu.cn); [ypan@zju.edu.cn](mailto:ypan@zju.edu.cn);

Contributing authors: [auhitayan@mail.scut.edu.cn](mailto:auhitayan@mail.scut.edu.cn);  
[21s053071@stu.hit.edu.cn](mailto:21s053071@stu.hit.edu.cn); [22132120@zju.edu.cn](mailto:22132120@zju.edu.cn); [langyuli@zju.edu.cn](mailto:langyuli@zju.edu.cn);

<sup>†</sup>These authors contributed equally to this work.

## Abstract

Ising annealer is a promising quantum-inspired computing architecture for combinatorial optimization problems. In this paper, we introduce an Ising annealer based on the Hamiltonian Monte Carlo, which updates the variables of all dimensions in parallel. The main innovation is the fusion of an approximate gradient-based approach into the Ising annealer which introduces significant acceleration and allows a portable and scalable implementation on the commercial FPGA. Comprehensive simulation and hardware experiments show that the proposed Ising annealer has promising performance and scalability on all types of benchmark problems when compared to other Ising annealers including the state-of-the-art hardware. In particular, we have built a prototype annealer which solves Ising problems of both integer and fraction coefficients with up to 200 spins on a single low-cost FPGA board, whose performance is demonstrated to be better than the state-of-the-art quantum hardware D-Wave 2000Q and similar to the expensive coherent Ising machine. The sub-linear scalability of the annealer

signifies its potential in solving challenging combinatorial optimization problems and evaluating the advantage of quantum hardware.

**Keywords:** Ising annealer, Hamiltonian Monte Carlo, Combinatorial optimization, Parallel computing, FPGA

## 1 Introduction

As a novel computing paradigm, quantum computing has the potential to vastly surpass its classical counterparts in solving challenging problems [Shor \(1994\)](#); [Grover \(1996\)](#). In particular, there may exist efficient quantum algorithms to solve the NP-hard combinatorial optimization problems [Farhi et al \(2014\)](#); [Albash and Lidar \(2018a\)](#); [Guerreschi and Matsuura \(2019\)](#); [Yan and Sinitzyn \(2022\)](#). For example, quantum approximation optimization algorithm (QAOA) and quantum annealing (QA) may help us reach the approximate solution faster [Albash and Lidar \(2018b\)](#); [Mandrà and Katzgraber \(2018\)](#).

Quantum annealers require precise hardware and environment control, which are expensive and may not be compatible with near-term quantum devices. Inspired by general quantum computing, many models of optical Ising machines and FPGA-based annealers have been proposed for combinatorial optimization [Wang et al \(2013\)](#); [Babaeian et al \(2019\)](#); [Mohseni et al \(2022\)](#); [Waidyasooriya and Hariyama \(2021\)](#); [Aadit et al \(2022\)](#); [Lu et al \(2023\)](#), including the famous optical coherent Ising machine (CIM) which treats the discrete Ising spins as continuous optical phases [Chou et al \(2019\)](#); [Vaidya et al \(2022\)](#); [Honjo et al \(2022\)](#). Ising annealers implemented with classical computing can also achieve a speedup based on hardware parallelism [Aadit et al \(2022\)](#); [Okuyama et al \(2019\)](#). To be more precise, the current classical Ising annealers are implemented on several CPUs or GPUs, and the optimal result is selected from the independent and parallelized optimization processes [Kowalsky et al \(2022\)](#); [Zhu et al \(2015\)](#); [Aramon et al \(2019\)](#).

For further speedup, simulated bifurcation algorithm [Goto et al \(2019\)](#); [Tatsumura et al \(2021\)](#); [Goto et al \(2021\)](#) and graph decoupling algorithm [Aadit et al \(2022\)](#) have been introduced for the simultaneous updating of the spins, which are also adapted to generic spin connections and non-binary coupling coefficients. However, the simulated bifurcation algorithm focuses on the Ising problems without local fields, while the graph decoupling algorithm introduces extra heuristic procedures for isolating the spins.

In this paper, we propose an Ising annealer implemented with a parallel algorithm, which is compatible with general types of spin connections and fixed-point coupling coefficients. This annealer is named as Parallel Hamiltonian Monte Carlo Ising Annealer, or PHIA. This annealer samples feasible configurations with a highly parallelized Hamiltonian Monte Carlo (HMC) method, which derives the candidates by sliding the sampling points on the energy landscape guided by the Hamiltonian equations. HMC [Neal \(2012\)](#) is proposed as an alternative for Gibbs sampler on continuous variables. The Gaussian augmented HMC (GAHMC) was introduced in [Pakman](#)

and Paninski (2013) to extend the vanilla HMC sampling to discrete variables. However, the gradient descent method has not yet been applied to GAHMC, which severely limits its efficiency. Therefore, we derive an extended GAHMC method to solve the Ising annealing problems with an approximate gradient-based method based on our previous research Li et al (2023). In our PHIA, the updating of a position variable is only dependent on its corresponding momentum variable, thereby guaranteeing the parallelized updating of all dimensions. The approximate gradient-based approach is then introduced into the annealing algorithm after the fusion of discrete Ising problem and the continuous HMC sampler for a further speedup. Finally, the max degree of parallelism is achieved by implementing the gradient-based HMC sampling procedure on a low-cost commercial FPGA board which can simulate up to hundreds of spins. We compare the PHIA with the state-of-the-art algorithms and hardware, including the simulated CIM Tiunov et al (2019), D-Wave 2000Q (DW2Q) and CIM Hamerly et al (2019); Goto et al (2021) on benchmark problems. The experiment results show that PHIA can achieve superb performance regardless of the problem type.

## 2 Results

### 2.1 Parallel anealer based on HMC

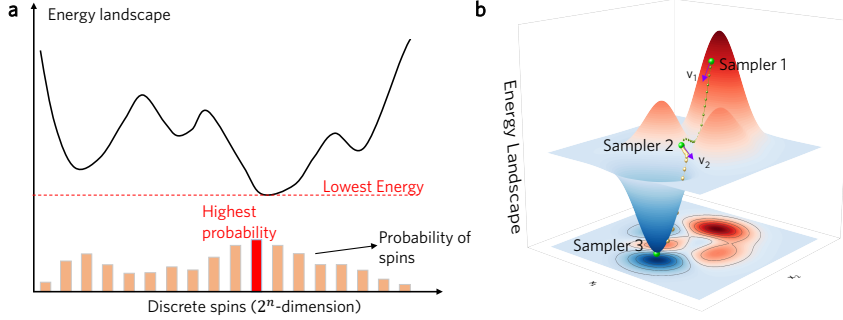


**Fig. 1** (a) The relation between the energy landscape of the Ising problem and the probability of spin configurations, where a low energy signifies a high sampling probability according to the Boltzmann distribution. (b) HMC method allows a particle to slide on the energy landscape. The final location of the particle is the candidate sampling point and the initial position of the next round of sampling.

The proposed PHIA is used to solve the combinatorial optimization problem. Like other Ising annealers, the optimization problem reduces to seeking for the ground states of an Ising Hamiltonian Lucas (2014).

The probability of obtaining a spin configuration  $\mathbf{s} \in \{-1, 1\}^n$  of an ensemble of  $n$  spins in the Ising model follows the Boltzmann distribution

$$p(\mathbf{s}) = \frac{1}{Z} \exp[-\beta E(\mathbf{s})], \quad (1)$$

where  $E(\mathbf{s})$  is the energy of the configuration with the normalization factor  $Z$ , and  $\beta$  is the inverse temperature. The relation between the energy landscape and the probability of spin configurations is shown in Fig. 1a. The energy landscape in Ising model is defined by the following Hamiltonian

$$E(\mathbf{s}) = - \sum_{i < j} J_{ij} s_i s_j - \sum_{i=1}^n h_i s_i, \quad (2)$$

where the spins are mutually coupled through the internal field  $J_{ij} \in \mathbb{R}$  and simultaneously affected by the local field  $h_i \in \mathbb{R}$ . The global minimum of Eq. (2) is the solution to the optimization problem.

The traditional Gibbs sampling method samples from the Ising Hamiltonian with an acceptance probability and updates only one spin in a single run, which severely limits its scalability in high-dimension problems. In contrast, as shown in Fig. 1b, HMC is a fundamentally different approach which proposes the candidate sampling points by evolving the Hamiltonian equations on the energy landscape and updating the variables of all dimensions in parallel. More specifically, the sampling point slides on the energy landscape with randomly initialized momentum  $\mathbf{v}$  at a certain position  $\mathbf{x}$ , governed by the Hamiltonian equations

$$\begin{cases} \dot{x}_i = \frac{\partial H}{\partial v_i}, \\ \dot{v}_i = -\frac{\partial H}{\partial x_i}, \end{cases} \quad (3)$$

with  $H(\mathbf{x}, \mathbf{v}) = U(\mathbf{x}) + K(\mathbf{v})$ . Here  $U(\mathbf{x})$  denotes the potential energy which corresponds to  $E(\mathbf{s})$  in the Ising model, and  $K(\mathbf{v}) = \frac{1}{2} \|\mathbf{v}\|_2^2$  is the kinetic energy. The Hamiltonian equations guarantee that in PHIA each pair of  $x_i$  and  $v_i$  can be updated in parallel.

The key result of this paper is the fusion of the gradient descent method for accelerating the HMC sampling process, based on the model proposed in [Pakman and Paninski \(2013\)](#) that converts the sampling of binary variables into the sampling of continuous variables for solving the Ising optimization problems. This is done by correlating the spin variables with the continuous position variables by a joint probability distribution  $p(\mathbf{s}, \mathbf{x})$ . By assuming that  $U(\mathbf{x})$ , which is the continuous counterpart of  $E(\mathbf{s})$ , also obeys the Boltzmann distribution  $p(\mathbf{x}) \propto \exp[-\beta U(\mathbf{x})]$ , we can derive the explicit form of  $H$  as

$$H(\mathbf{x}, \mathbf{v}) = \beta E(\text{sgn } \mathbf{x}) + \frac{1}{2} \mathbf{x}^T \mathbf{x} + \frac{1}{2} \mathbf{v}^T \mathbf{v}. \quad (4)$$

**Table 1** Main Logic Resources on the ALINX-AX7Z100

Device	Slice Registers	LUT	DSP	LUTRAM
ALINX-AX7Z100	554,800	277,400	2020	108,200

More details about this derivation can be found in Appendix A. Then the Hamiltonian equations are calculated as

$$\begin{cases} \dot{x}_i = v_i, \\ \dot{v}_i = \beta \frac{d(\text{sgn } x_i)}{dx_i} I(\text{sgn } x_i) - x_i, \end{cases} \quad (5)$$

with

$$I(\text{sgn } x_i) = - \left. \frac{\partial E(\mathbf{s})}{\partial s_i} \right|_{\mathbf{s}=\text{sgn } \mathbf{x}} = \sum_{j=1}^n J_{ij}(\text{sgn } x_j) + h_i. \quad (6)$$

The exact solution to the Hamiltonian equations can be obtained by considering the zero-cross of the continuous variables [Pakman and Paninski \(2013\)](#), whereas an iterative gradient descent ‘leapfrog’ method [Neal \(2012\)](#) will be more friendly for parallel implementation on the FPGA. However in our case, since  $\text{sgn } x_i$  is non-differentiable, we have to invoke the following approximation

$$\text{sgn } x_i \approx \text{Tanh}(\gamma x_i), \quad (7)$$

$$\frac{d}{dx_i} \text{Tanh}(\gamma x_i) = \gamma [1 - \text{Tanh}^2(\gamma x_i)], \quad (8)$$

with a hyper-parameter  $\gamma$  for the gradient calculation. The HMC sampling gives the current estimate of  $\mathbf{x}^*$  minimizing  $U(\mathbf{x})$ . Therefore, the corresponding spin configuration  $\mathbf{s}^*$  calculated by  $\mathbf{s}^* = \text{sgn } \mathbf{x}^*$  is the current estimate that minimizes  $E(\mathbf{s})$ . The ground states of the Ising Hamiltonian can be found by repeating this sampling process.

## 2.2 The FPGA implementation of the parallel annealer

FPGA [Kilts \(2007\)](#) is an integrated circuit with configurable logic blocks that admit parallel execution. In this paper, ALINX-AX7Z100 FPGA board is used for demonstration. Table 1 shows the characteristics of ALINX-AX7Z100. The implementation is based on the fixed-point arithmetic, which extends the solvable problems to Ising Models with non-integer  $J_{ij}$  and  $h_i$ .

Speed and area are the main considerations in the logic design [Koç and Paar \(1999\)](#). In our implementation, increased logic resources are used for the loop unrolling in each iteration to accelerate the annealing process. In addition, at the cost of larger circuit size, pipeline is used to improve parallelism, and sharing blocks between different operations reduces the consumption of time and resources. There are two main shared blocks which calculate Eq. (4) and Eq. (5) as shown in Fig. 2a and Fig. 2b, respectively. The parameters for the internal field  $J_{ij}$  and local field  $h_i$  are stored in Read Only Memory (ROM). In Fig. 2b, FUNC1 and FUNC2 can work in parallel as there is

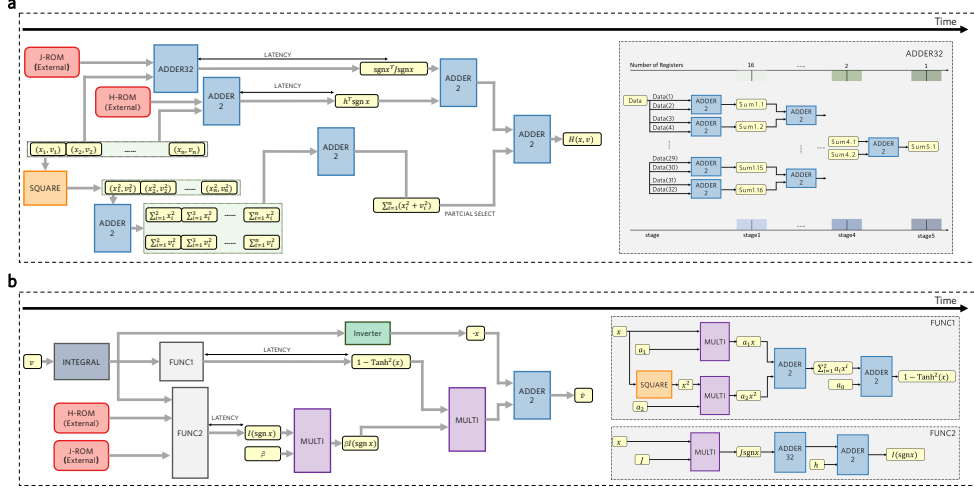


**Fig. 2** Schematic of two main blocks in the FPGA implementation. (a) The block that calculates  $H(\mathbf{x}, \mathbf{v})$ . ADDER32 is a 5-stage pipelined logical block composed of 31 ADDER2s. (b) The block that calculates  $\dot{v}$ . The main latency originates from computing the derivative of the sign function and Eq. (6).

no data dependency between them. With the pipeline design, the updating of  $\mathbf{x}$  and  $\mathbf{v}$ , which is the most time-consuming part of the calculation, can be significantly shortened. Note that we adopt a quadratic polynomial approximation to Eq. (8) which only takes 2 MULTIs, 2 ADDER2s and 1 SQUARE. Additional control circuitry such as finite state machine (Appendix B) is required to organize the logic blocks.

## 3 Numerical results

### 3.1 Problem definition for benchmark experiments

Next, we present a number of benchmark experiments in which different types of combinatorial optimization problems are considered. The definition of these problems is summarized in Table 2. The maxcut problems, including maxcut\_d3 and maxcut\_dense, are aimed at finding the optimal partition of a given unweighted graph Hamerly et al (2019). The sk problems, including sk\_bool, sk\_ising, and sk\_uniform, are aimed at computing the ground states of the Sherrington-Kirkpatrick spin glass model with different types of coupling coefficients Sherrington and Kirkpatrick (1975); Hamerly et al (2019). The nae\_3\_sat problem is a variant of the satisfiability problem Oshiyama and Ohzeki (2022). The spin\_model is an Ising problem whose coupling coefficients are randomly chosen from the uniform distribution. In particular, coupling coefficients in both sk\_uniform and spin\_model are float-point numbers, while coefficients in the other problems are not.

**Table 2** Datasets and Parameters for Benchmarking

problem	internal $J_{ij}$	external $h_i$
maxcut_dense	$\{0, 1\}$	0
maxcut_d3	$\{0, 1\}$	0
sk_bool	$\{0, 1\}$	0
sk_ising	$\{-1, +1\}$	0
sk_uniform	0 or $U(0, 1)$	0
nae_3_sat	$\{0, \pm 1, \pm 2, \dots, \}$	0
spin_model	$U(-1, 1)$	$U(-1, 1)$

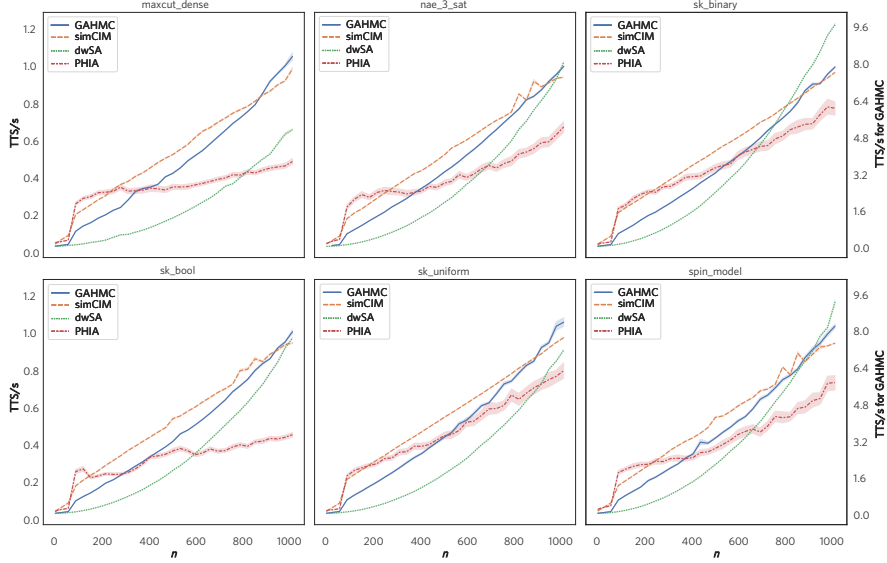


**Fig. 3** The simulation results on different Ising annealers. With the dimension of the problem grows, the PHIA outperforms the other Ising annealers on all types of problems. The TTSs of the GAHMC are much larger than the other annealers, and thus are indicated with a different axis on the right with a different scale.

### 3.2 The simulation of the parallel annealer

Ising annealers in general do not guarantee that the global optimum can be obtained. Hence, we employ the Time-To-Solution (TTS) as the performance index to quantify the expected time to attain the best solution with a ninety nine percent confidence [King et al \(2015\)](#). The optimal solution is estimated using the third-party Python library ‘dwave-neal’ ([dwSA](#)) [dwa \(2022\)](#). TTS is defined by

$$\text{TTS} = T_1 \left[ \frac{\lg(1 - 0.99)}{\lg(1 - P)} \right], \quad (9)$$

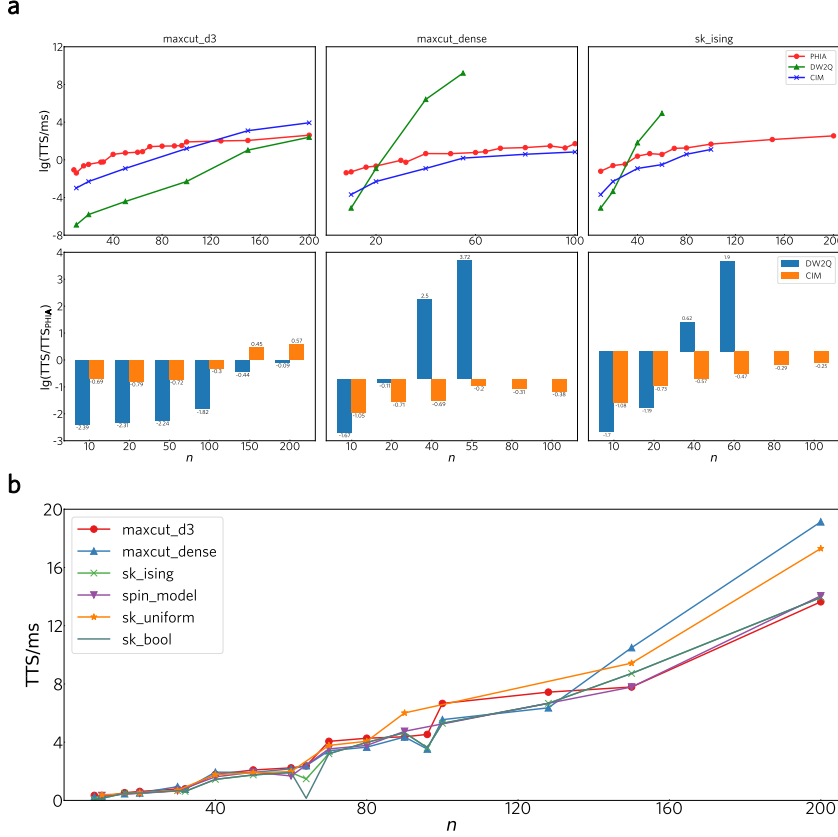


**Fig. 4** Data of CIM and DW2Q are borrowed from [Hamerly et al \(2019\)](#). (a) The comparison of TTS on 3 types of problems.  $\text{TTS}_{\text{PHIA}}$  is the TTS of PHIA. (b) Performance of PHIA on various combinatorial optimization problems.

where  $T_1$  is the time of a single run, and  $P$  is the probability of finding the ground state within a single annealing. Fig. 3 depicts the average time to approach the optimal solutions for various combinatorial optimization problems as the dimension of problems grows.

In our experiments, all types of optimization problems are firstly converted into Ising annealing problems. In each type of problem, 100 instances with dimension that scales from 8 to 1024 are tested to evaluate the scalability of four annealers on the same CPU (AMD Ryzen 7 5800H at 3.20 GHz with 16-GB memory) in Python. The simulated annealer ‘dwSA’ is implemented by directly calling the API provided by ‘dwave-neal’, and the simulations of coherent Ising machine ‘simCIM’ and ‘GAHMC’ are implemented using Python according to the algorithm designs in [Pakman and Paninski \(2013\)](#). As shown in Fig. 3, the PHIA outperforms the other three annealers on all six types of problems when the problem size increases beyond 800. In particular, it can be observed that the TTS of GAHMC is at least 8 times larger than the other annealers, which demonstrates the huge advantage of our proposed PHIA



over the vanilla GAHMC without using the gradient descent. Moreover, dwSA surges exponentially and the simCIM rises linearly as the dimension increases. In contrast, the PHIA obeys a sub-linear growth law, which demonstrates its superb scalability in high dimensions.

### 3.3 Demonstration of the parallel annealer on FPGA

There exists a significant difference between fraction and integer calculation in the logic circuit design, where integer calculation often consumes more resources and time. The benchmark problems listed in Table 2 can be divided into integer ones and fractional ones depending on whether the internal  $J_{ij}$  and external  $h_i$  are integers. PHIA can deal with both problems.

We compare the FPGA-based PHIA against DW2Q and CIM in Fig. 4a. It should be noted that DW2Q and CIM are specifically designed for optimization problems with integer coefficients, and thus we are constraining the capability of our device in order to make a comparison on the small subset of problems that can be solved using the FPGA-based PHIA. CIM and DW2Q have shown that they can be faster than the classical counterparts, depending on the type of the problem. Due to the hardware constraints, they can also be slower. For example, the performance of DW2Q is not satisfying on maxcut problem with dense connections, since the hardware does not directly support the implementation of dense connections. In contrast, the PHIA maintains a stable sub-linear growth in running time for different problem types. In Appendix B, we have given an estimate of the time for a single run on the FPGA, which clearly shows that the running time of PHIA will not grow exponentially with the problem size. Note that CIM has achieved similar performance, at the expense of complex optical equipment.

In addition to the integer problems, the PHIA achieves stable and satisfying performance on the fractional problems, which is demonstrated in Fig. 4b.

## 4 Discussion and conclusion

We have proposed a scalable heuristic annealing algorithm based on HMC sampling for solving the Ising problems. The gradient-based approach has been fused into the previous plan which introduces significant acceleration and facilitates parallel processing. Due to the simultaneous updating of each dimension, we have demonstrated a significant increase in scalability and built a prototype annealer that solves Ising problems with up to 200 spins on a single FPGA.

The proposed annealer outperforms its counterparts in various benchmark problems as the problem size increases. When implemented with a single FPGA, the annealer also achieves a satisfying performance when compared with the state-of-the-art hardware CIM and DW2Q on optimization problems with integer coefficients. In addition, the proposed hardware is adapted to both integer and fraction problems. Therefore, this annealer could serve as the benchmark to measure the performance of quantum hardware.

Due to the sub-linear growth of the execution time of the PHIA, it is promising to consider multi-FPGA systems for developing an ultrafast solver that is compatible with

Ising problems of thousands of spins, which corresponds to large-scale combinatorial optimization problems that is still challenging in classical computing.

## Appendix A Implementation details of the Ising annealer via the discrete HMC sampler

In HMC, the physically inspired Hamiltonian is defined using the continuous variables  $\mathbf{x}$  and  $\mathbf{v}$ . HMC guarantees the conservation of total energy and an acceptance probability of 1 for the sampling points Neal (2012), while the probability of rejection in the traditional Monte Carlo sampling is nonzero.

However, the energy function in Eq. (2) is defined over binary variables which are incompatible with the continuous HMC. Here we have used the approach proposed in Pakman and Paninski (2013) to convert the sampling of binary spins into the sampling of continuous distributions, which is detailed as follows.

Assume the joint probability distribution of the continuous variables  $\mathbf{x}$  and the discrete variable  $\mathbf{s}$  is written as

$$p(\mathbf{s}, \mathbf{x}) = p(\mathbf{s})p(\mathbf{x} | \mathbf{s}). \quad (\text{A1})$$

The conditional probability is set as Pakman and Paninski (2013)

$$p(\mathbf{x} | \mathbf{s}) = g(\mathbf{x})\delta(\text{sgn } \mathbf{x} - \mathbf{s}), \quad (\text{A2})$$

with  $g(\mathbf{x})$  being a continuous function that can be arbitrarily chosen. It can be proved that  $g(\mathbf{x})$  is a probability distribution. Therefore, a trivial choice for  $g(\mathbf{x})$  is

$$g(\mathbf{x}) = (2/\pi)^{n/2} \exp\left(-\frac{1}{2}\mathbf{x}^T \mathbf{x}\right). \quad (\text{A3})$$

In this case, the marginal probability distribution  $p(\mathbf{x})$  can be derived as

$$p(\mathbf{x}) = p(\mathbf{s} = \text{sgn } \mathbf{x})g(\mathbf{x}). \quad (\text{A4})$$

According to the Boltzmann distribution  $p(\mathbf{x}) \propto \exp[-\beta U(\mathbf{x})]$ , the potential energy is given by

$$\begin{aligned} \beta U(\mathbf{x}) &= -\ln[p(\mathbf{x})] \\ &= -\ln[p(\mathbf{s} = \text{sgn } \mathbf{x})] - \ln[g(\mathbf{x})] \\ &= \beta E(\text{sgn } \mathbf{x}) + \frac{1}{2}\mathbf{x}^T \mathbf{x} + C(\beta), \end{aligned} \quad (\text{A5})$$

with  $C(\beta)$  being a constant. Since a constant factor does not affect the value of  $\mathbf{x}$  that minimizes  $U(\mathbf{x})$ , the Hamiltonian  $H(\mathbf{x}, \mathbf{v})$  can be formulated as

$$H(\mathbf{x}, \mathbf{v}) = \beta E(\text{sgn } \mathbf{x}) + \frac{1}{2}\mathbf{x}^T \mathbf{x} + \frac{1}{2}\mathbf{v}^T \mathbf{v}. \quad (\text{A6})$$

**Table B1** The behaviors of states.

States	Behavior
1	Initialization
2	Updating $v$ in the first iteration
3	Executing the rest iterations of the EM algorithm
4	Calculating the acceptance rate and adjusting the temperature of the annealing algorithm
5	Determining whether the PHIA has obtained the optimal solution and saving the best result achieved so far

Then the sampling on  $U(\mathbf{x})$  can be conducted by simulating the Hamiltonian equations Eq. (5), using the Leapfrog numerical integration method as outlined in Neal (2012). In particular,  $\mathbf{x}$  and  $\mathbf{v}$  are updated by using an approach similar to the expectation-maximization (EM) algorithm

$$\begin{cases} \mathbf{x}^{(i+1)} = \mathbf{x}^{(i)} + \epsilon \mathbf{v}^{(i)}, \\ \mathbf{v}^{(i+1)} = \mathbf{v}^{(i)} - \epsilon \nabla H(\mathbf{x}^{(i+1)}), \end{cases} \quad (\text{A7})$$

where  $\epsilon$  controls the step size of each update, and  $\nabla H(\mathbf{x})$  denotes the gradient of  $H$  in the  $\mathbf{x}$  direction

$$\nabla H(\mathbf{x}) = \frac{\partial H}{\partial \mathbf{x}}. \quad (\text{A8})$$

## Appendix B Estimation of the time for a single run on the FPGA

The global clock frequency of the FPGA board is 100 MHz. The annealing process is planted into the FPGA as a state machine of 5 states. The states are listed in Table B1.

One clock cycle (Clk) serves as the unit to measure the time taken by each state

$$\text{Clk} = \frac{1}{100 \text{ MHz}} = 10 \text{ ns}. \quad (\text{A9})$$

The time cost by the State 1 is approximately

$$T_{s1} = \left(\frac{n}{2} + 5\right) \text{Clk}. \quad (\text{A10})$$

The time cost by the State 2 is about

$$T_{s2} = \left(\frac{n}{2} + 10 + (n+2)\lfloor \frac{n}{32} \rfloor\right) \text{Clk} \quad (\text{A11})$$

The time for a single run is mainly consumed in repeating the gradient update procedures for  $L$  times in State 3, which is denoted by  $T_{s3}$ .  $T_d$  is the latency caused by the

Block shown in Fig. 2b, which constitutes the major part of  $T_{s3}$ .  $T_d$  is calculated by

$$T_d = (n + 12 + (n + 2)\lfloor \frac{n}{32} \rfloor) \text{ Clk}, \quad (\text{A12})$$

where  $\lfloor \cdot \rfloor$  denotes the Greatest Integer Function. Then  $T_{s3}$  is given by

$$\begin{aligned} T_{s3} &= LT_d + L(13 + n) \\ &= L(2n + 25 + (n + 2)\lfloor \frac{n}{32} \rfloor) \text{ Clk}. \end{aligned} \quad (\text{A13})$$

The time for a single run is estimated as

$$\begin{aligned} T_{\text{est}} &= T_{s1} + T_{s2} + T_{s3} \\ &= ((2L + 1)n + 15 + 25L + \\ &\quad (L + 1)((n + 2)\lfloor \frac{n}{32} \rfloor)) \text{ Clk}, \end{aligned} \quad (\text{A14})$$

which clearly indicates that the running time will not grow exponentially with the problem size  $n$ .

## Declarations

### Funding

This work was supported by the National Key R&D Program of China (Nos. 2022YFB3304700 and 2022YFB3103100) and the National Natural Science Foundation of China (Nos. 62173296 and 62273154).

### Availability of data and materials

The data and materials that support the findings of this study are available from the corresponding author upon reasonable request.

## References

- (2022) Dwave neal documentation. Available at <https://docs.ocean.dwavesys.com/-/downloads/neal/en/latest/pdf/>
- Aadit NA, Grimaldi A, Carpentieri M, et al (2022) Massive parallel probabilistic computing with sparse Ising machines. *Nat Electron* 5:460–468. <https://doi.org/10.1038/s41928-022-00774-2>
- Albash T, Lidar DA (2018a) Adiabatic quantum computation. *Rev Mod Phys* 90(1):015002. <https://doi.org/10.1103/RevModPhys.90.015002>

- Albasha T, Lidar DA (2018b) Demonstration of a scaling advantage for a quantum annealer over simulated annealing. *Phys Rev X* 8(3):031016. <https://doi.org/10.1103/PhysRevX.8.031016>
- Aramon M, Rosenberg G, Valiante E, et al (2019) Physics-inspired optimization for quadratic unconstrained problems using a digital annealer. *Front Phys* 7:48. <https://doi.org/10.3389/fphy.2019.00048>
- Babaeian M, Nguyen DT, Demir V, et al (2019) A single shot coherent Ising machine based on a network of injection-locked multicore fiber lasers. *Nat Commun* 10:516. <https://doi.org/10.1038/s41467-019-11548-4>
- Chou J, Bramhavar S, Ghosh S, et al (2019) Analog coupled oscillator based weighted Ising machine. *Sci Rep* 9:14786. <https://doi.org/10.1038/s41598-019-49699-5>
- Farhi E, Goldstone J, Gutmann S (2014) A quantum approximate optimization algorithm. Preprint at <https://arxiv.org/abs/1411.4028>
- Goto H, Tatsumura K, Dixon AR (2019) Combinatorial optimization by simulating adiabatic bifurcations in nonlinear Hamiltonian systems. *Sci Adv* 5(4):eaav2372. <https://doi.org/10.1126/sciadv.aav2372>
- Goto H, Endo K, Suzuki M, et al (2021) High-performance combinatorial optimization based on classical mechanics. *Sci Adv* 7(6):eabe7953. <https://doi.org/10.1126/sciadv.abe7953>
- Grover LK (1996) A fast quantum mechanical algorithm for database search. In: *Proc. 28th Annu. ACM Symp. Theory Comput.* Association for Computing Machinery, New York, NY, USA, pp 212–219, <https://doi.org/10.1145/237814.237866>
- Guerreschi GG, Matsuura AY (2019) QAOA for Max-Cut requires hundreds of qubits for quantum speed-up. *Sci Rep* 9:6903. <https://doi.org/10.1038/s41598-019-43176-9>
- Hamerly R, Inagaki T, McMahon PL, et al (2019) Experimental investigation of performance differences between coherent Ising machines and a quantum annealer. *Sci Adv* 5(5):eaau0823. <https://doi.org/10.1126/sciadv.aau0823>
- Honjo T, Sonobe T, Inaba K, et al (2022) 100,000-spin coherent Ising machine. *Sci Rep* 7(40):abh0952. <https://doi.org/10.1126/sciadv.abh0952>
- Kilts S (2007) *Advanced FPGA Design: Architecture, Implementation, and Optimization.* John Wiley & Sons, Hoboken
- King J, Yarkoni S, Nevisi MM, et al (2015) Benchmarking a quantum annealing processor with the time-to-target metric. Preprint at <https://arxiv.org/abs/1508.05087>

- Koç ÇK, Paar C (1999) Cryptographic Hardware and Embedded Systems: First International Workshop, CHES'99 Worcester, MA, USA, August 12-13, 1999 Proceedings. Springer Science & Business Media, Berlin
- Kowalsky M, Albash T, Hen I, et al (2022) 3-regular three-XORSAT planted solutions benchmark of classical and quantum heuristic optimizers. *Quantum Sci Technol* 7(2):025008. <https://doi.org/10.1088/2058-9565/ac4d1b>
- Li L, Wang H, Xie Z, et al (2023) Simulated Ising annealing algorithm with Gaussian augmented Hamiltonian Monte Carlo. In: Proc. 42nd Chin. Control Conf. IEEE, Tianjin, PRC, pp 6760–6765, <https://doi.org/10.23919/CCC58697.2023.10240679>
- Lu B, Fan CR, Liu L, et al (2023) Speed-up coherent Ising machine with a spiking neural network. *Opt Express* 31(3):3676–3684. <https://doi.org/10.1364/OE.479903>
- Lucas A (2014) Ising formulations of many NP problems. *Front Phys* 2:5. <https://doi.org/10.3389/fphy.2014.00005>
- Mandrà S, Katzgraber HG (2018) A deceptive step towards quantum speedup detection. *Quantum Sci Technol* 3(4):04LT01. <https://doi.org/10.1088/2058-9565/aac8b2>
- Mohseni N, McMahon PL, Byrnes T (2022) Ising machines as hardware solvers of combinatorial optimization problems. *Nat Rev Phys* 4:363–379. <https://doi.org/10.1038/s42254-022-00440-8>
- Neal RM (2012) MCMC using Hamiltonian dynamics. Preprint at <https://arxiv.org/abs/1206.1901>
- Okuyama T, Sonobe T, Kawarabayashi K, et al (2019) Binary optimization by momentum annealing. *Phys Rev E* 100(1):012111. <https://doi.org/10.1103/PhysRevE.100.012111>
- Oshiyama H, Ohzeki M (2022) Benchmark of quantum-inspired heuristic solvers for quadratic unconstrained binary optimization. *Sci Rep* 12:2146. <https://doi.org/10.1038/s41598-022-06070-5>
- Pakman A, Paninski L (2013) Auxiliary-variable exact Hamiltonian Monte Carlo samplers for binary distributions. In: Proc. Adv. Neural Inf. Process. Syst., p 26, URL [https://proceedings.neurips.cc/paper\\_files/paper/2013/hash/a7d8ae4569120b5bec12e7b6e9648b86-Abstract.html](https://proceedings.neurips.cc/paper_files/paper/2013/hash/a7d8ae4569120b5bec12e7b6e9648b86-Abstract.html)
- Sherrington D, Kirkpatrick S (1975) Solvable model of a spin-glass. *Phys Rev Lett* 35:1792. <https://doi.org/10.1103/PhysRevLett.35.1792>
- Shor PW (1994) Algorithms for quantum computation: discrete logarithms and factoring. In: Proc. 35th Annu. IEEE Symp. Found. Comput. Sci., pp 124–134,

<https://doi.org/10.1109/SFCS.1994.365700>

- Tatsumura K, Yamasaki M, Goto H (2021) Scaling out Ising machines using a multi-chip architecture for simulated bifurcation. *Nat Electron* 4:208–217. <https://doi.org/10.1038/s41928-021-00546-4>
- Tiunov ES, Ulanov AE, Lvovsky A (2019) Annealing by simulating the coherent Ising machine. *Opt Express* 27(7):10288. <https://doi.org/10.1364/OE.27.010288>
- Vaidya J, Kanthi RSS, Shukla N (2022) Creating electronic oscillator-based Ising machines without external injection locking. *Sci Rep* 12:981. <https://doi.org/10.1038/s41598-021-04057-2>
- Waidyasooriya HM, Hariyama M (2021) Highly-Parallel FPGA accelerator for simulated quantum annealing. *IEEE Trans Emerg Topics Comput* 9(4):2019–2029. <https://doi.org/10.1109/TETC.2019.2957177>
- Wang Z, Marandi A, Wen K, et al (2013) Coherent Ising machine based on degenerate optical parametric oscillators. *Phys Rev A* 88(6):063853. <https://doi.org/10.1103/PhysRevA.88.063853>
- Yan B, Sinitsyn NA (2022) Analytical solution for nonadiabatic quantum annealing to arbitrary Ising spin Hamiltonian. *Nat Commun* 13:2212. <https://doi.org/10.1038/s41467-022-29887-0>
- Zhu Z, Ochoa AJ, Katzgraber HG (2015) Efficient cluster algorithm for spin glasses in any space dimension. *Phys Rev Lett* 115(7):077201. <https://doi.org/10.1103/PhysRevLett.115.077201>